Spatially–resolved heterogeneous dynamics in a strong colloidal gel

Stefano Buzzaccaro, Matteo David Alaimo, Eleonora Secchi, and Roberto Piazza

Department of Chemistry, Chemical Engineering and Material Science (CMIC), Politecnico di Milano, via Ponzio 34/3, 20133 Milano, Italy

Abstract. We reexamine the classical problem of irreversible colloid aggregation, showing that the application of Digital Fourier Imaging (DFI), a class of optical correlation methods that combine the power of light scattering and imaging, allows to pick out novel useful evidence concerning the restructuring processes taking place in a strong colloidal gel. In particular, the spatially-resolved displacement fields provided by DFI strongly suggest that the temporally-intermittent local rearrangements taking place in the course of the gel ageing are characterized by very long-ranged spatial correlations.

Keywords: colloidal aggregation; gels; disordered solids; dynamic light scattering; digital microscopy; velocimetry; correlation spectroscopy.

Submitted to: *J. Phys.: Condens. Matter*

1. Introduction

The irreversible aggregation processes induced in suspensions of charged particles by the addition of destabilizing electrolytes are among the first and more extensively investigated subjects in colloidal science [1, 2, 3]. The long experimental and theoretical journey leading from the earlier basic surveys of the aggregation kinetics to the detailed analysis of the structures these processes generate is spangled with landmark results, which allowed for instance to unravel the structural and dynamic properties of fractal clusters, or to pinpoint subtle analogies with other diffusion-driven physical effects like spinodal decomposition [1]. Besides providing copious and fruitful insights to non-equilibrium statistical physics, these studies, and in particular those addressing the space-spanning structures eventually produced by colloidal aggregation, fostered the development of novel experimental and theoretical tools suitable to investigate the origin and nature of more complex arrested structures, ranging from repulsive and attractive glasses to tenuous depletion gels. On the practical side, understanding colloidal aggregation processes has provided an important spin-off in the industrial

manipulation and transport of disperse systems and in the development of materials with unparalleled mechanical and thermal properties such as the aerogels.

As a matter of fact, one is tempted to question whether novel relevant chapters may be added to this already successful story. Yet, it is exactly the extensive efforts recently performed to scrutinize the structure and dynamics of arrested colloidal structured which suggests that the well-established field of irreversible colloidal aggregation may worth be reexamined. Depletion gels and colloidal glasses display indeed complex ageing processes, characterized by a spatially and temporally heterogenous dynamics, often accompanied by sudden local restructuring event that rule the long-time mechanical and rheological behavior of these structures. Several very general features of these processes have already been singled out, first by standard Dynamic Light Scattering (DLS, [3]) and then, more recently, by Time Resolved Correlation (TRC, [4]), a clever approach that, besides being immune from the annoying problems deriving from the non-ergodic character of the light scattered by arrested colloids, provides novel and extremely useful evidence. Remarkably, the time-correlation functions of a wide class of disordered structures, which includes not only colloidal gels and glasses, but also foams and concentrated emulsions, share a similar "two-step" relaxation, characterized by an initial and relatively well understood fast decay, due to the thermally activated motion of particles in the cage formed by their neighbors [5] or to the thermally excited internal elastic modes of the gel [2, 6], followed by a much slower and more intriguing relaxation that, depending on the system, may display ballistic [3, 7, 6], diffusive [8], subdiffusive [9], or even hyperdiffusive [10] features. Although understanding the detailed mechanisms underlying these surprisingly diverse kinds of dynamical behavior is challenging, an increasing consensus is emerging about the pivotal role played by the relaxation of frozen internal stresses that build up during the gelation process [6, 11].

If we restrict our discussion to the specific case of the tenuous gels made of particles strongly bound by dispersion forces that form in irreversible colloidal aggregation, several more features can be singled out:

(i) The static structure factor $S(q)$ shows a peak at finite q that, while aggregation proceeds, grows in amplitude and shift towards smaller q-vectors. This behaviour, resembling what is observed in spinodal decomposition processes, is the signature of the growth of large fractal clusters that eventually merge into an interconnected gel network [1]. Over much longer times scales the "hole" at small q progressively fills up, eventually yielding a monotonically decreasing $S(q)$ [3].

(ii) The gel dynamics, though almost arrested and just due to intermittent rearrangement events associated to small local particle displacements, is nevertheless correlated over long spatial scales [12].

(iii) As already mentioned, the intensity time-correlation functions display a two-step decay, with the slowest relaxation showing a compressed exponential behaviour $g(\tau) = \exp\left[-(\tau/\tau_r)^p\right]$, with $p \simeq 1.5$ in the limit $q \to 0$, and a correlation time τ_r that scales as q^{-1}, instead of q^{-2} as in standard diffusive processes [7, 6].

Whereas standard scattering methods have provided a detailed picture of the *overall* properties of irreversible colloidal gels, information about the occurrence of static and dynamic spatial heterogeneity effects in these structure is still rather poor. Recent investigation of soft glasses [13] and biopolymer networks [11], prove instead that spatially-resolved measurements can be extremely useful to test basic models of arrested system dynamics. For instance, the simplest model [6] capable of accounting for the experimental findings i)–iii) is based on assuming that the rearrangement events underlying the relaxation dynamics are independent (hence distributed along the time axis as a Poisson) and that each one, although taking place locally, generates a long-ranged dipolar elastic displacement field affecting the whole scattering volume [12]. A further more delicate assumption is that, on the length scales probed by the scattering experiments, the displacements due to two subsequent events take place along the same direction. This is a reasonable ansatz provided that the two events originate from the same stress source (assumed to require several events to fully relax), that the stress sources are very diluted, and that their life time exceeds the relaxation time of the system. While the first two assumptions are supported by TRC measurements, the last one requires real-space imaging of the long-ranged displacement field over, which is hard to perform with bright field or confocal microscopy because the requirement to resolve single particle motion necessarily limits the field of view.

In the present work, we show that the application to the study of irreversible colloid aggregation of Differential Fourier Imaging (DFI) methods [14], a novel class of optical correlation techniques combining the power of scattering and microscopy, sheds new light on irreversible aggregation, arguably one of the most extensively investigated processes in colloidal science. In fact the results we present, besides providing evidence on the evolution in time of the structure factor, on sample aging and temporal heterogeneity, and on the behavior of the correlation functions that are fully consistent with those already obtained by DLS and TRC techniques, allow for a detailed analysis of the displacement field, which confirm that rearrangement events are long-ranged and that consecutive local displacements occur on average along the same direction. After a brief presentation of the experimental method and setup, the paper is organized in two sections, separately discussing the evidence obtained from a real and a reciprocal space analysis, so to emphasize the complementary information that can be obtained using DFI methods.

2. Differential Fourier Imaging: blending microscopy with dynamic light scattering

When it comes to unravel and characterize the rich dynamics of arrested colloidal systems, most of the traditional experimental strategies successfully applied to investigate colloid aggregation prove to be rather powerless. On the one hand, both DLS and TRC cannot pinpoint localized events, because of their spatial averaging feature; on the other, direct imaging through a microscope, although suitable to detect single local

rearrangements, misses the intrinsic statistical averaging property of scattering methods required for a profitable use of spatial and temporal correlation concepts. In the past few years, however, the strong demand for novel experimental approaches allowing to probe the peculiar gel and glass dynamics has fostered the development of several ingenious optical correlation methods joining the powers of scattering and imaging methods. At the roots of these techniques is the common strategy of collecting the intensity pattern in a plane sufficiently close to the sample (more formally, within the so-called "deep Fresnel" diffraction region [14]). Seminal experiments by Giglio *et al.* [15, 16] have indeed shown that in this "near-field" condition the speckle pattern stemming from the interference between the transmitted and scattered fields contains, at variance with the far field speckle distribution (just fixed by the geometry of the scattering volume), full information about the size and spatial distribution of the scatterers. This is easily accomplished provided that minimal requirements on the *spatial* coherence properties of imaging optics are met, for instance by simple stopping down with a diaphragm the illumination source. It is important to notice that, even in a standard imaging configuration, where we nominally map just the *sample* plane on the detector, the latter nevertheless collects near-field scattering too, because of the finite depth of focus of the image-forming optics.

One of the crucial advantages of this general approach is that it is highly flexible for what concerns sample illumination: any radiation source, like a spectral lamp [17, 18], a LED [19], or even a x-ray source [20, 21], whose spatial coherence is suitably controlled (for instance, by stopping-down its emitting aperture with a simple diaphragm) works perfectly. Provided that the amount of scattered light is weak compared to the incident one, moreover, the intrinsic heterodyne detection scheme of the technique (field-mixing of the transmitted and scattered radiation) ensures that the imaging formation method is linear space invariant (LSI). This means that the intensity captured by the sensor can be written as a convolution integral of the form [14]

$$i(\mathbf{r},t) = i_0(\mathbf{r}) + \int dz \int d\mathbf{r} T(\mathbf{r}-\mathbf{r}',z) c(\mathbf{r}',z,t), \tag{1}$$

where $\mathbf{r}$ and z are, respectively, the coordinates perpendicular and parallel to the optical optical axis, $T(\mathbf{r},z)$ is the 3D point spread function of the system, $c(\mathbf{r},z)$ is the local sample concentration, and $i_0(\mathbf{r})$ is a purely instrumental, time invariant background contribution. Eq. (1) is of primary importance: indeed, linear space invariance ensures that the Fourier power spectrum of the detected intensity distribution $i(\mathbf{r},t)$ is nothing but the structure factor of the investigated sample, multiplied by a transfer function that accounts for the details of the experimental setup [21, 14]. If the transfer function is known, the technique yields both the structural information obtained in static small-angle light scattering experiments and, from the q-resolved temporal correlation of the Fourier transform of $i(\mathbf{r},t)$, the dynamic properties of the system usually derived from DLS experiments.

It is worth noticing that, in principle, LSI can also be obtained by exploiting other optical properties of the sample besides scattering (for instance, if the sample is

fluorescent of partially absorbing [22]), or by generating intensity modulations by phase contrast methods. However, in the absence of a *coherent* superposition between the transmitted and the scattered field, temporal fluctuations in the image plane just reflect particle *number* fluctuations within a coherence area of the illuminating source. Hence, these alternative approaches are not particularly suited to investigate concentrated particle suspensions, where number fluctuations are quenched. Nevertheless, all heterodyne and incoherent imaging techniques where a faithful series of images is the sample is first collected, and then digitally elaborated so to extract *a posteriori* the time-behaviour of each single Fourier component, can be collected under the common name of Digital Fourier Imaging (DFI) ‡. All of them, indeed, besides allowing to investigate inhomogeneous samples by simply dividing the image in different Regions of Interest (ROIs) that are separately analyzed according to the method we sketched, can accurately map, through the analysis of the spatial cross correlations between different images, the local displacements within a sample that is due either to external stresses such as gravity or mechanical shear [23], or, even in the absence of an external field, to spontaneous internal restructuring events.

Although DFI techniques have originally addressed colloids showing a stationary dynamics, nothing prevents from applying them to investigate systems displaying ageing effects and a temporally heterogeneous dynamics. The basic trick consists in isolating via software each specific wave-vector using a digital bandpass filter, starting from a collected stack of images, and then in analyzing the time-behavior of each Fourier component separately. This approach yields the same kind of spatially-resolved information obtained by Photon Correlation Imaging (PCI) [12, 19], a related technique combining TRC [4] with imaging, with the further advantage that no physical mask in the focus plane of the imaging optics is required. Besides, since this Fourier analysis is made *a posteriori*, DFI measurements retain the whole real-space information of standard imaging, therefore allowing to contrast the evidence obtained from direct visualization with that stemming from a reciprocal space analysis.

2.1. Bright Field DFI

The former general considerations are further specified in this Section to a heterodyne DFI setup operating in bright field, which simply requires to illuminate the scattering medium with a source having sufficiently high spatial coherence and to detect with a multi-pixels sensor (usually a CMOS) the intensity pattern on a plane close to the sample. As we already mentioned, the total field on such a plane is given by the superposition of the scattered field E_s with the transmitted unscattered field E_t. The intensity (or better, the irradiance) detected by the sensor is therefore:

$$\mathrm{i}(\mathbf{r},\mathrm{t}) \propto |E(\mathbf{r},t)|^2 = |E_t|^2 + 2\mathrm{Re}(E_t^* E_s) + |E_s|^2. \qquad (2)$$

‡ An equivalent denomination would be “Digital Fourier Microscopy”, although the imaging optics may not necessarily be that of a microscope. In fact, the configuration used in this work resembles more a large “spyglass” than a microscope.

Under the assumption of weak scattering, the last term in Eq. 2 can be neglected (*heterodyne detection*), and the LSI condition expressed by Eq. 1 is satisfied because $E_s \propto c(\mathbf{r}, z, t)$. In the following, we shall try to highlight the main information that can be extracted either from a direct manipulation of a time–sequence of bright-field DFI images, or from a reciprocal–space analysis of their 2-D Fourier transform.

a) Real Space. If all the relevant length scales of the physical system under investigation can be optically resolved, standard video microscopy provides of course a direct way to detect local displacements of an elastic or plastic structure, the velocity field of flowing colloids, or even the hydrodynamic motion of a simple fluid seeded with tracer particles, as in Particle Imaging Velocity (PIV). As we already mentioned, however, direct tracking suffers from a major drawback when the size of investigated structures is close to the optical resolution limit. In fact, the high numerical aperture (NA) microscope objectives required to image them necessarily have a limited field of view, which does not allow investigating displacements or motion that are correlated over much larger spatial scales. Conversely, it is exactly when considering the opposite case of system whose microscopic structure *cannot* be resolved, but still generate refractive index fluctuations that scatter a non-negligible amount of light, that the power of DFI fully emerges. However small, indeed, the scattered field is consistently "pumped up" by heterodyning with the transmitted field, so that the intensity distribution on a plane downline of the scattering cell displays weak modulations, which fluctuate in time, over a strong flat background. The latter can furthermore be removed, if necessary, either by taking the difference between two subsequent images, or by subtracting out the intensity distribution obtained by averaging over a sufficiently long time. The time-evolution of this rather dull, weak speckle pattern nevertheless contains all the information needed to reconstruct physical displacements in the sample.

To see this, consider first as a simple example a suspension of particles lying within a thin layer perpendicular to the optical axis, and undergoing a rigid in-plane displacement $\Delta\mathbf{R}$ in a time δt. Neglecting for the moment the effect of Brownian motion, the image generated at time $t + \delta t$ is simply related to the image at time t by a rigid spatial translation by $\Delta\mathbf{R}$. Hence, when mapped as a function of the displacement vector $\Delta\mathbf{R}$, the time-correlation function of the normalized intensity [24, 18]

$$G_{\mathbf{r},t}(\Delta\mathbf{R}; \delta t) = i(\mathbf{r}, t) i(\mathbf{r} + \Delta\mathbf{R}, t + \delta t)$$

displays a well defined cross-correlation peak, whose shift between different images allows to obtain $\Delta\mathbf{R}$. Random thermal motion modifies this simple picture by inducing a spreading in time and a corresponding decrease in amplitude of the correlation peak. This scheme, quite similar to the approach used in PIV has been recently exploited to design a novel technique, "Ghost Particle Velocimetry" (GPV), which allows obtaining the flow pattern in microfluidic devices [18], or to monitor sedimentation effects in colloidal gels subjected to the gravitational stress [23].

b) Reciprocal Space. A Fourier analysis of the images provides the link between standard DLS and DFI measurements, hence allowing DFI to probe the local microscopic dynamics of the sample. Before expatiating of this, it is however worth discussing a delicate but important issue. Scattering measurements are arguably the most powerful tool in condensed matter because they provide direct structural and dynamic information of length scales comparable to the inverse of the scattering wave-vector $\mathbf{q}$, the difference between the wave-vectors of the incident and scattered radiation: For instance, the static structure factor $S(\mathbf{q})$ is simply related to the *three*-dimensional Fourier transform of the two-point spatial correlation function. Conversely, a *two*-dimensional transform on the image plane yields only the *projection* $\mathbf{q}_{\shortparallel} = (q_x, q_y)$ of $\mathbf{q}$, and provides no information on the perpendicular component q_z. This means that the structure factor obtained by taking the Fourier transform of the intensity distribution on the image plane is not a fully faithful representation of $S(\mathbf{q})$, because $|\mathbf{q}_{\shortparallel}| < |\mathbf{q}|$. Besides, no motion along the optical axis can be detected. However, because in the paraxial approximation $q = (4\pi/\lambda)\sin(\theta/2) \simeq k\theta$, where θ is the scattering angle and λ the wavelength in the medium, we have

$$q^2 \simeq q_{\shortparallel}^2 \left[1 + \left(\frac{q_{\shortparallel}}{2k}\right)^2\right], \tag{3}$$

so that the perpendicular component of $\mathbf{q}$ is $q_z \simeq q_{\shortparallel}^2/2k$ [25]. The second term in square brackets is of order θ, hence it is negligible for small scattering angles. From now on, therefore, we shall assume $|\mathbf{q}_{\shortparallel}| \simeq |\mathbf{q}|$, dropping the subscript. All quantities such as correlation functions and index obtained from the 2-D analysis in the image plane, moreover, will be assumed to coincide with the corresponding quantities defined in conventional light scattering.

More formally, it is convenient to introduce the 2-D Fourier transform of Eq. (1)

$$\widehat{i}(\mathbf{q}, t) = \widehat{i}_0(\mathbf{q}) + \int dq_z \widetilde{T}(\mathbf{q}, q_z)\widetilde{c}(\mathbf{q}, q_z, t), \tag{4}$$

which, for isotropic samples, allows to define, in full analogy with what is done in TRC [4], the so-called "correlation index"

$$C_1(q, \tau; t) = \left\langle \widehat{i}(\mathbf{q}, t+\tau)\widehat{i}^*(\mathbf{q}, t) \right\rangle_q, \tag{5}$$

where $\langle \ldots \rangle_q$ is an ensemble average over a ring at constant $q = |\mathbf{q}|$, and its normalized form

$$c_1(q, \tau; t) = \frac{C_1(q, \tau; t)}{\sqrt{C_1(q, 0; t) C_1(q, 0; t+\tau)}}. \tag{6}$$

Notice that the correlation index is a function of the "delay time" τ, whereas t is just a parameter specifying that correlations may explicitly depends on the "ageing time" after sample preparation.

For the following discussions it is also useful to introduced a "q-averaged" correlation index, directly evaluated in the real space by averaging over all the image

pixels

$$C^i(\tau,t) = \frac{\langle i(\mathbf{r},t)i(\mathbf{r},t+\tau)\rangle}{\langle i(\mathbf{r},t)\rangle\langle i(\mathbf{r},t+\tau)\rangle} - 1, \tag{7}$$

with the normalized form $c^i(\tau,t) = C^i(\tau,t)/C^i(0,t)$. Using Parseval's theorem, $C^i(\tau,t)$ can be shown to be formally related to the q-dependent correlation index in Eq. (5) by

$$C^i(\tau,t) = \frac{\int_0^\infty 2\pi q C_1(q,\tau,t)dq}{\sqrt{C_1(0,0,t)C_1(0,0,t+\tau)}} - 1. \tag{8}$$

For a fixed value of τ, a drop in $c^i(\tau,t)$ plotted versus t physically indicates the occurrence (somewhere within the sample) of restructuring events in the course of sample ageing.

If the dynamics is stationary, or changes very slowly with t, $C_1(q,\tau;t)$ and $c_1(q,\tau;t)$ can be averaged over a suitably short time interval Δt to obtain the *intermediate scattering function* $G_1(q,\tau) = \langle C_1(q,\tau,t)\rangle_{\Delta t}$ and its normalized version $g_1(q,\tau)$. Quite generally, the link between G_1 and g_1 can be written as

$$G_1(q,\tau) = N|T(q)|^2 S(q) g_1(q,t) + B(q) \tag{9}$$

where N is total number of particles and $B(q)$ a background contribution taking in account other possible sources of noise [21]. Because $g_1(\tau) \to 0$ for $\tau \to \infty$, $G_1(q,\tau)$ asymptotically approaches the background contribution $B(q)$, allowing to subtract it out. Moreover, since $g_1(0) = 1$,

$$G_1(q,\tau;0) = N|T(q)|^2 S(q) + B(q).$$

Hence, an accurate calibration of the optical setup with a suspension of very small particles where $S(q) \simeq 1$ allows to measure the transfer function of the system.

Notice that, because of the heterodyne condition, $g_1(\tau)$ is actually a *field* (1st order) time-correlation function, which is sensitive also to *absolute* (and not just to relative) displacements of the scatterers. For instance, in the case of translation with a constant velocity $\mathbf{V}_0$, the image intermediate scattering function is a pure imaginary quantity $G_1(\mathbf{q},\tau) = \exp(\imath\mathbf{q}\cdot\mathbf{V}_0\tau)$. The decorrelation of the speckle field due to an overall sample motion of this kind, which may originate from sedimentation effects or vibration of the setup, can mask the internal intrinsic rearrangements of the sample that we want to probe. To avoid these spurious effects, it is worth considering instead the 2nd order correlation function

$$G_2(q,\tau) = \left\langle \left\langle \widehat{i}(q,t+\tau)\widehat{i}^*(q,t+\tau)\widehat{i}(q,t)\widehat{i}^*(q,t) \right\rangle \right\rangle_{\Delta t}. \tag{10}$$

(with $\langle\langle \ldots \rangle\rangle$ indicating that both a statistical and time average must be taken), or its normalized form

$$g_2(q,\tau) = G_2(q,\tau)/G_2(q,0),$$

which is the Fourier transform of the power spectrum of the intensity distribution, and coincides with the intensity correlation function measured by homodyne DLS techniques in a far field configuration.

3. Experimental

3.1. Colloidal system

We have investigated monodisperse polystyrene latex spheres with a diameter of 98 nm and a refractive index $n = 1.59$, dispersed at a volume fraction $\phi \simeq 2.9 \times 10^{-4}$, which is sufficiently low to avoid multiple scattering effects, in a $H_2O - D_2O$ mixture whose composition is adjusted to match the particle density, so to hinder sedimentation effects. Colloidal aggregation is induced by bringing the concentration of $CaCl_2$ to a value $c = 16\,\mathrm{mM}$. Because this divalent salt concentration is just above the critical flocculation value, the aggregation kinetics proceeds sufficiently slow to be conveniently monitored. The suspension is then rapidly poured into an optical cuvette with a cross-section $2\,\mathrm{mm} \times 10\,\mathrm{mm}$, which is filled up to a height of 20 mm.

3.2. Optical setup

The setup used in this investigation is a slight modification of the apparatus described in [23]. The illumination is provided by a high-power red-light LED ($\lambda = 625\,\mathrm{nm}$, Smart Vision Lights, USA), smoothed out by a ground glass. The source is limited in size by a pinhole with a diameter $D = 1.5\,\mathrm{mm}$ to enhance the degree of spatial coherence, and placed in the rear focus of a lens that turns it into a parallel beam with a diameter of about 25 mm and a transversal spatial coherence length of about $30\,\mu\mathrm{m}$, which illuminates the sample, contained in a thin quartz cuvette with an optical path of 2 mm. A 8.7× magnified image of the sample is formed on the CMOS camera (Hamamatsu Orca-Flash 4.0, 2048×2048 square px. of side $6.5\,\mu\mathrm{m}$) by an achromatic doublet of focal length $f = 30\,\mathrm{mm}$, yielding an effective field of view on the cell central plane of about $1.5\,\mathrm{mm} \times 1.5\,\mathrm{mm}$, with each pixel on the camera corresponding to a demagnified region on the sample of about $0.75\,\mu\mathrm{m} \times 0.75\,\mu\mathrm{m}$. This optical configuration has a transfer function that allows to probe accurately a wave-vector range $0.03\,\mu\mathrm{m}^{-1} < q < 1\,\mu\mathrm{m}^{-1}$, corresponding to scattering angles $0.2° \leq \theta \leq 6°$. The optical axis of the apparatus is set orthogonally to the direction of gravity with an accuracy of $\pm 1°$.

3.3. Spatially-resolved measurements

The strategy adopted to derive spatially-resolved measurements of the displacement pattern is basically borrowed from PIV, where coarse-grained velocity fields are obtained by splitting the images in ROIs, and analyzing then spatial cross-correlations between images of the same ROI taken a suitable time interval δt apart [24, 18, 23]. Choosing the size of a ROI necessarily requires coming to an arrangement between the contrasting requirements of a good spatial resolution, which of course increases with the number of ROIs, and of a sufficient statistical accuracy, which improves with the ROI size. For the system we investigated, a reasonable tradeoff was choosing square ROIs of 160 pixels in side, yielding for each image a coarse-grained displacement field made of set of 12×12 vectors. A time-step $\delta t = 60\,\mathrm{s}$ was found to be fully adequate to follow the microscopic

dynamics during the whole course of aggregation and of the following gel ageing, if exception is made of local-mode relaxation processes taking place at very short time.

4. Structure and "global" dynamics of strong colloidal gels

4.1. Time-evolution of the gel structure

To obtain a faithful reconstruction of the temporal evolution of the static structure factor $S(\mathbf{q};t)$ of the suspension, a detailed knowledge of the transfer function $T(\mathbf{q})$ of the specific imaging configuration is mandatory. In general $T(\mathbf{q})$ depends not only on the characteristics of optical instrument, such as the numerical aperture NA of the illumination and of imaging optics and the degree of temporal coherence of the source, but also on several properties of the sample, like the complex refractive index of the suspension, or the thickness and position of the cell. The simplest way to obtain $T(\mathbf{q})$ consists in calibrating the optical system by means of a known reference sample. To this aim, we have used a dilute solution of fluorinated particles with a radius of 90 nm, which ensure that, to a good approximation, both the structure factor and the form factor are constant within the investigated small-q range. It is also important to take into account that, during the aggregation process, the scattered intensity increases by more than an order of magnitude. Hence, although the scattered field remains weak with respect to the transmitted one, so that the heterodyne condition is still fulfilled, changes in the transmitted intensity in the course of gelation are not negligible. To account for this effect, the intensity distribution within each of the images taken at different gelation time is normalized to its spatial average. The static background can then be safely removed from the time-sequence of normalized images by subtracting out their temporal average, and the power spectrum $S(\mathbf{q};t)$ is obtained by dividing the normalized, background subtracted images by $T(\mathbf{q})$. Due to the isotropy of the system, $S(\mathbf{q};t)$ can be finally radially averaged to improve the signal statistics of the signal.

Fig.1, where the radially-averaged structure factor is plotted for several values of the time t from the beginning of the aggregation process (the "ageing time" t), confirms that $S(q;t)$ shows a peak at a finite value of q, which in time grows and shifts towards smaller q-values. Simultaneously, $S(0;t)$ progressively grows until, after about 1 day, the hole at small q is completely filled. In the later stage, all curves display at large q an approximate power-law decay with an exponent close to 1.7, which is consistent with the fractal dimension of a gel forming by Diffusion Limited Cluster Aggregation (DLCA). Reassuringly, this spinodal-like evolution of the structure function, is fully consistent with what has already been found in several SALS studies of irreversible aggregation in similar colloidal systems [1, 3].

4.2. Global dynamics and temporal heterogeneity

As shown in Fig. 2, where we plot the normalized q-averaged correlation index $c^i(\tau;t)$ for three values of the delay time τ, the gel microscopic dynamics slows down in time.

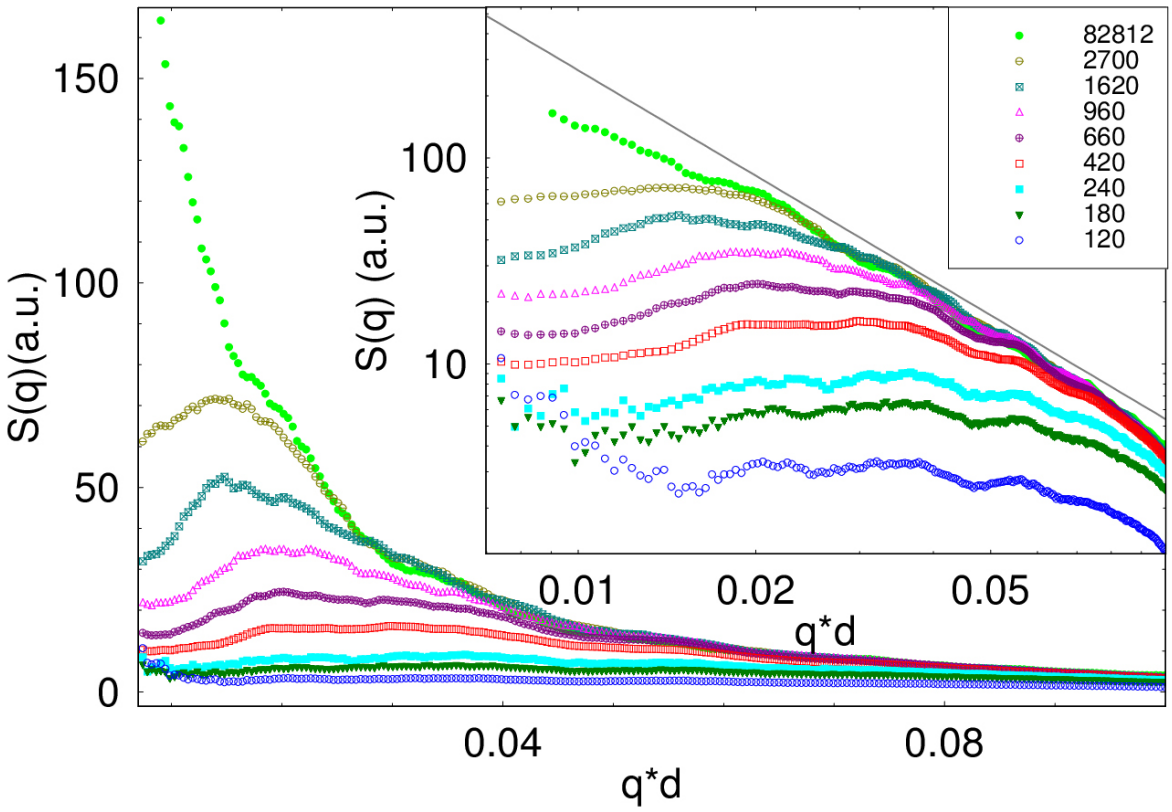

Figure 1. Main: Time-evolution of the static scattered intensity. Each curves is labelled in the legend by the ageing time t in seconds. The same data are shown on a log-log plot in the inset, where the continuous line is a power law decay with exponent 1.7.

Actually, when the ageing time t is larger than about 10^4 s, the correlation between the initial speckle pattern and a speckle pattern taken with a delay time $\tau = 60$ s is almost complete, which means that, over the time scale of a minute, the gel dynamics is basically arrested§. For much larger delay times, a progressive decrease of $c^i(\tau;t)$ is nevertheless observed, to the point that, for $\tau \gtrsim 10$ minutes, the correlation between two subsequent speckle patterns vanishes regardless of the age of the gel: physically, this means that, over very long times, the gel slightly "creeps". On top of this overall increasing behavior, however, $c^i(60\,\mathrm{s};t)$ displays sudden and "spiky" drops, with a duration comparable or shorter than than the minimum delay from two consecutive frames of 60 s, corresponding to abrupt changes in the speckle pattern, which arguably stem from local rearrangement events in the gel‖.

In the following, we focus on the time window $6 \times 10^4\,\mathrm{s} \leq \Delta t \leq 8 \times 10^4\,\mathrm{s}$, shown by

§ Full correlation ($c^i(\tau;t) = 1$) is never reached, however, because of the fast internal relaxation modes of the gel, which cause a decay of $5 - 10\%$ of the correlation functions over very short time.

‖ We recall that, as mentioned in Section 2.1, the correlation index shown in Fig. 2 resumes the contribution of all detected q-vectors. In principle, however, a q-resolved correlation index could be obtained by analyzing the images in the Fourier space. Yet, this time-consuming analysis is arguably not essential at the general level of discussion we choose.

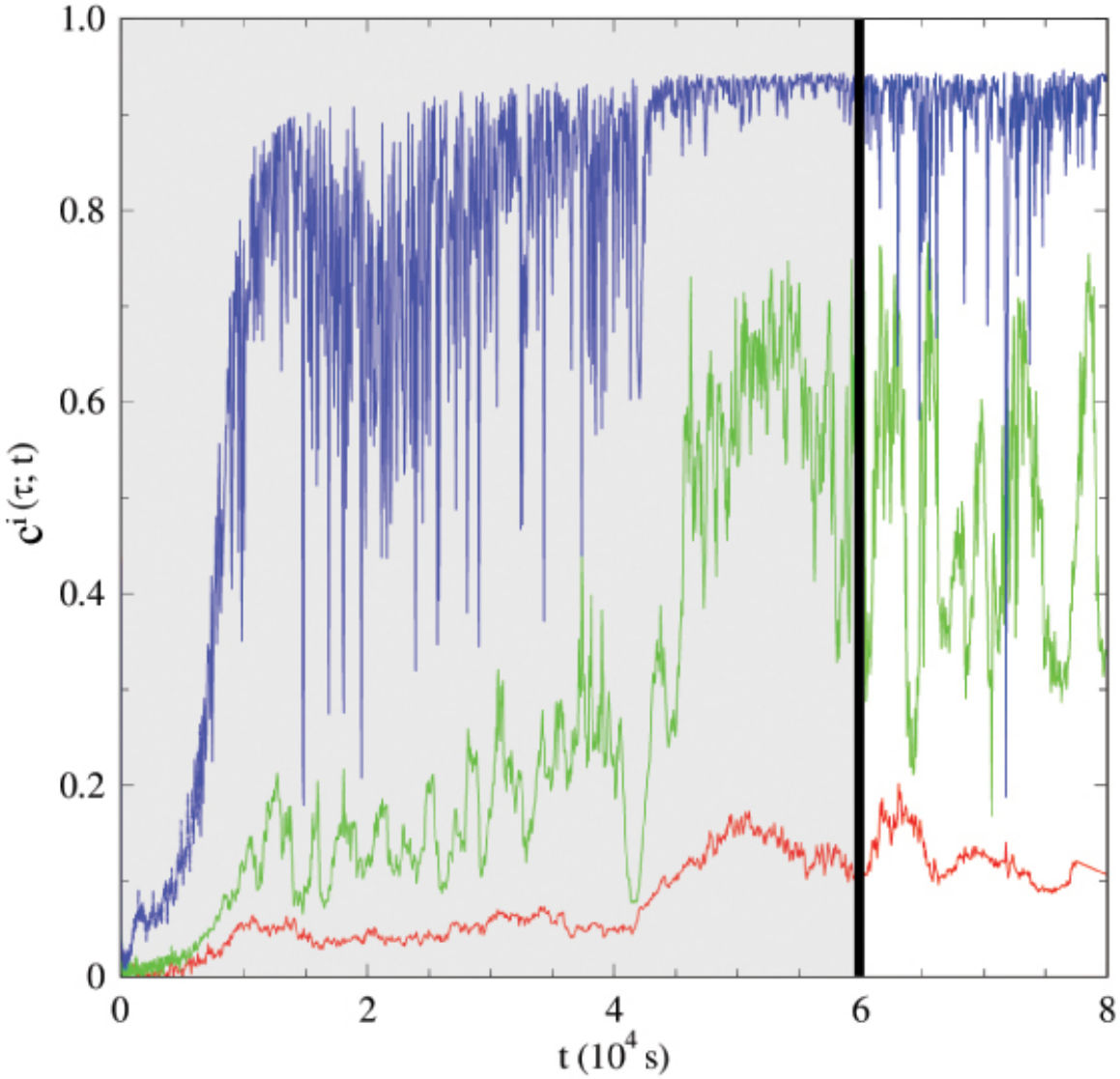

Figure 2. Time-evolution of $c^i(\tau;t)$ at delay times $\tau = 60$, 1200, and 6000 s (from top to bottom). The vertical line shows the lower limit of the interval Δt used to obtain $g_2(q,\tau)$.

the box in Fig. 2, where the most relevant part of the gel ageing has already taken place. The top panel in Fig. 3 shows that, after a short-time decay too fast to be followed with our setup, the time-averaged correlation functions $g_2(q,\tau)$, obtained from the power spectra and plotted for several values of q, display a much slower relaxation which is quite well fitted by a compressed exponential decay

$$g_2(q,\tau) - 1 = a\mathrm{e}^{-(\tau/\tau_r)^p},$$

where a, τ_r and p depend on q. The compression exponent p, in particular, is found to decrease from approximately 1.5 at the smallest q we probed to a value slightly lower than 1 for the highest spatially frequency we proved (data not shown). Since

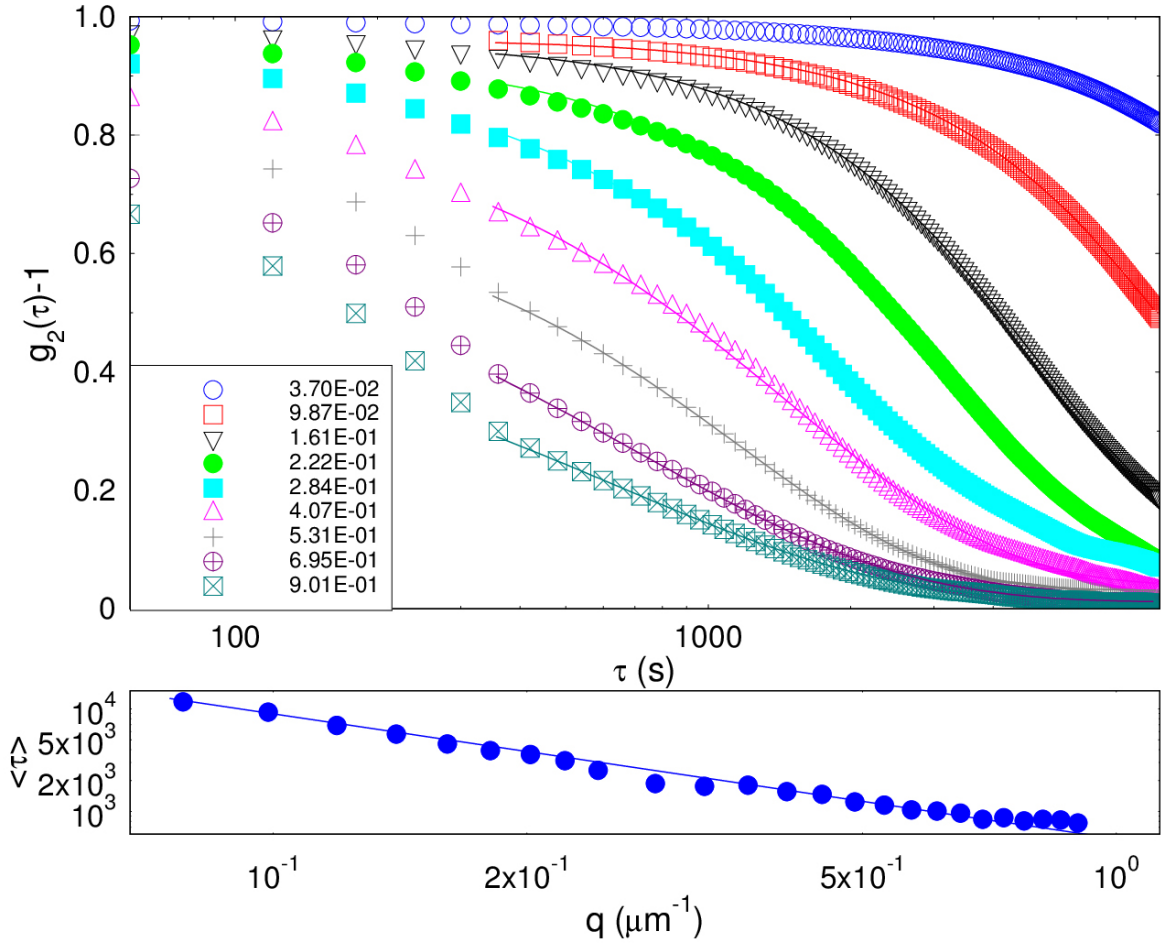

Figure 3. Top: Correlation functions at several q vectors, varying from $0.037\,\mu\mathrm{m}^{-1}$ (top curve) to $0.9\,\mu\mathrm{m}^{-1}$ (bottom curve). Full lines are compressed exponential fits to the long-time relaxation of $g_2(q,\tau)-1$. Bottom: double-log plot of the mean relaxation time $\langle\tau(q)\rangle$, fitted with a power law of exponent -1.2.

the overall shape of $g_2(q,\tau)$, fixed by p, is therefore wave-vector dependent, τ_r cannot strictly be regarded as an indicator of the typical decay time of the correlation function. The latter is better expressed by the time-integral $\langle\tau\rangle$ of $a^{-1}(g_2(q,\tau)-1)$, which, for a compressed (or stretched) exponential, is given by $\langle\tau\rangle = p^{-1}\Gamma\left(p^{-1}\right)\tau_r$, where Γ is the Euler gamma function. The bottom panel in Fig. 3 shows that $\langle\tau\rangle \propto q^{-1.2}$, suggesting a quasi-ballistic dependence of the relaxation time on q. These results are altogether in very good agreement with the previous findings by Duri *et al.* [6], with the only exception of the anomalously low value found for the p exponent at high q. So far, we have not found a sound explanation of this discrepancy, which may however just be a spurious effect due to the difficulty of subtracting the background at higher q, where the signal to noise ratio is lower.

The results presented in this Section confirm that DFI can be profitably used to obtain results that combine those obtained in static and dynamic light scattering

measurements using a single setup setups. Besides, the abrupt and highly intermittent events detected on top of a smooth slowing-down of the dynamics are in qualitative agreement with the picture provided by TRC. In the next Section, however, we show how an investigation in the real space can give further valuable information on these restructuring events which is not easily accessible to other techniques.

5. Spatial heterogeneity and displacement fields

The origin of the sudden and short-lived collapses in the correlation index observed in Fig. 2 is fully unraveled by a real-space analysis of the image differences, performed, as discussed in Section 3, by splitting the full field of view into 12×12 square ROIs. As before, we focus only on the gel behavior at long-time ($t > 6 \times 10^4$ s). Fig. 4 shows that the general behavior of the *mean* values of the displacement components $\Delta y(t), \Delta x(t)$ along and perpendicular to $\mathbf{g}$ (chosen along the negative y-axis) strongly resembles that of $c^i(t)$. For the largest fraction of the considered values of t (spaced, we recall, by 60 s), both components are indeed negligible. As the matter of fact, their average values over the whole time interval $6 \times 10^4\,\mathrm{s} < t < 8 \times 10^4\,\mathrm{s}$ are given by $\langle \Delta x \rangle_t = +0.07 \pm 0.04\,\mu$m and $\langle \Delta y \rangle_t = +0.12 \pm 0.02\,\mu$m. This amounts to an overall r.m.s. displacement of the gel by less of 0.5% over a period of more than 5 hours. Besides, the small net displacement along y takes places *against* the direction of gravity: we can then safely conclude that, thanks to the good density-matching conditions, sedimentation, at least for what concerns overall settling effects, is fully negligible. Remarkably, significant fluctuations are observed only in correspondence to de-correlation bursts, showing that the latter are in fact due to an overall tiny. displacement of the gel. Rather curiously, however, the fluctuations with respect to the mean along x are more than three times larger than along y.

A closer look to the detailed spatial distribution of the two displacement fluctuations, in particular if we contrast the behavior detected in correspondence to the strongest de-correlation burst ($t = t_2$ in Fig. 4) with that observed for a typical "still" condition ($t = t_1$). The scatter plot of the whole distribution of $\Delta x, \Delta y$ in the left panel of Fig. 5 shows indeed that to the strong de-correlation burst are associated much larger fluctuations over the different ROIs. Once again, a rather marked asymmetry between the horizontal and the vertical components is evident: whereas $\overline{\Delta y}_{t=t_2} \ll \overline{\Delta x}_{t=t_2}$, for the standard deviation we conversely have $\sigma_y \gg \sigma_x$. Namely, spatial fluctuations along y are much stronger than along x. The two histograms at the right side of Fig. 5, where the distributions of the standard deviations σ_x,σ_y over the whole investigated ageing period are contrasted, show that this is not an accidental feature associated to t_2, but rather a general signature of the displacement fluctuations. Spotting the origin of this peculiar behavior is rather challenging. A tentative explanation may be that gravity effects, although too weak to significantly influence the overall gel structure, may still have a symmetry-breaking effect by affecting the local fluctuations of the microscopic rearrangements: Yet, the data we have so far collected are not sufficient to adequately

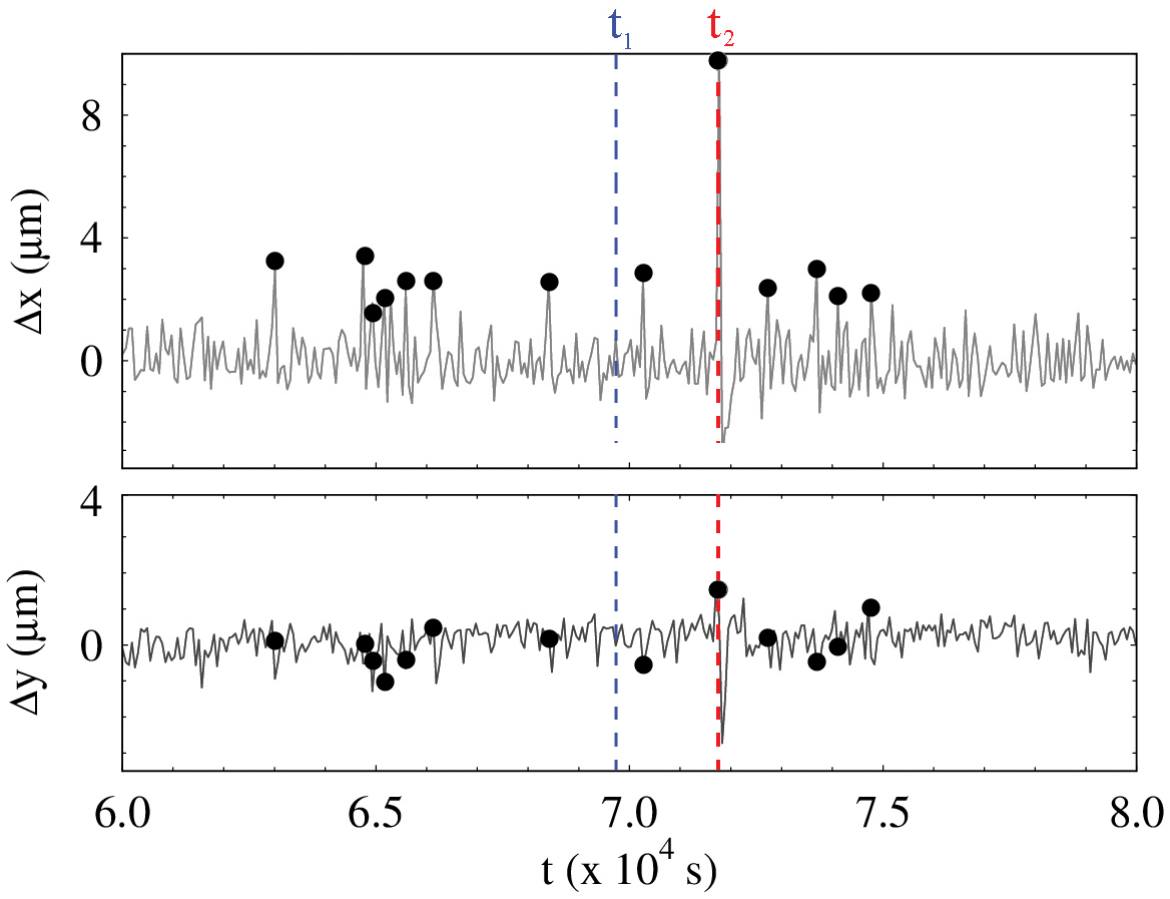

Figure 4. Average displacements perpendicular to (Δx, upper panel) and along (Δy, lower panel) gravity at late ageing time ($6 \times 10^4\,\mathrm{s} < t < 8 \times 10^4\,\mathrm{s}$). The dots over each curve mark the values of t where the correlation coefficient in Fig. 2 falls down to a value $c^i(60;t) \leq 0.8$.

support this claim, or to provide a clue for a consistent explanation of the observed asymmetry.

The most interesting evidence comes however from considering *correlations* between Δx and Δy. As a matter of fact, inspection of the data presented in Fig. 4 may suggest that these correlation are rather weak. By averaging over the *whole* set of values of t, we obtain indeed a rather small negative correlation coefficient¶

$$r(\Delta x, \Delta y) = \frac{\langle \Delta x - \langle \Delta x \rangle \rangle \langle \Delta y - \langle \Delta y \rangle \rangle}{\sigma_x \sigma_y} \simeq -0.1$$

On the *average*, therefore, orthogonal displacements are barely correlated. This picture drastically change, however, if we just focus on the instants where a consistent drop in the correlation coefficient is observed. Indeed, the two examples presented in the top part in Fig. 6 show that, within the displacement field associated to a de-correlation

¶ Notice that here we consider averages and standard deviations over t of the *mean* values of the displacements shown in Fig. (4).

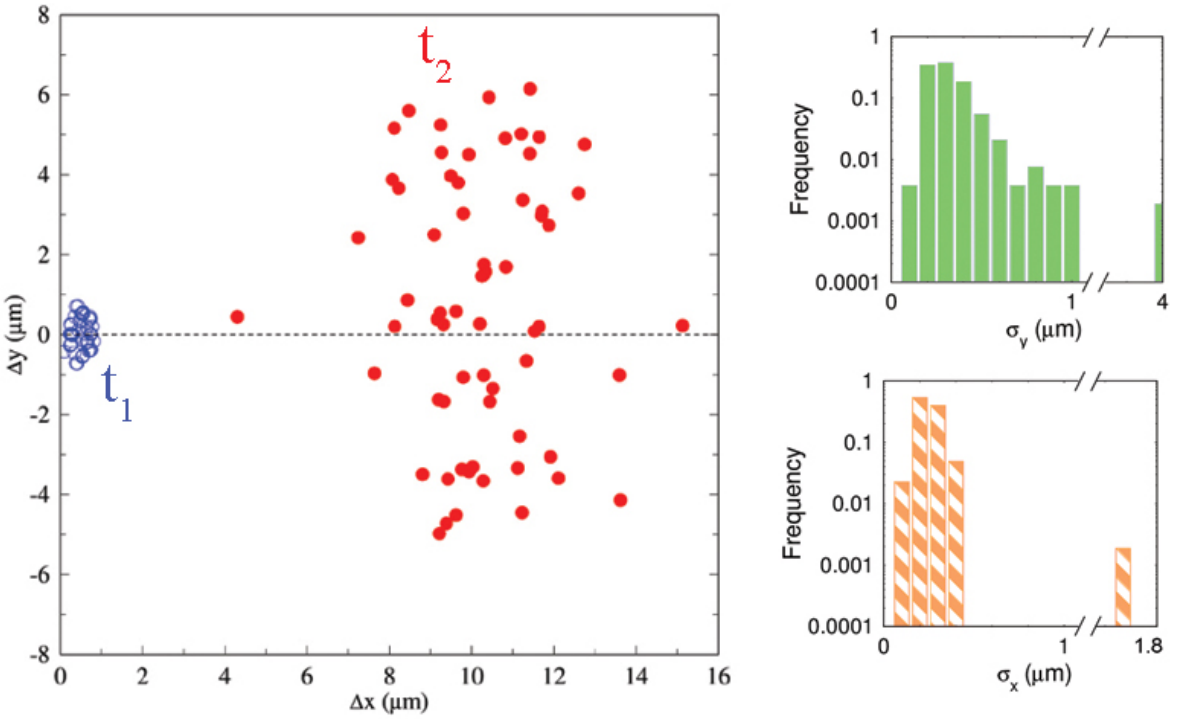

Figure 5. Left Panel: Scatter plot for the values of the displacement components at times t_1 and t_2 indicated by the dashed lines in Fig. 4. The full distribution of the standard deviations of the x and y components over the 144 ROI's over the whole investigated late-stage ageing period are shown by the histograms at the right.

event, the x and y components of the displacement field conversely display strong and spatially long-ranged correlations, with the overall displacement pattern resembling a kind of instantaneous "eddy". Besides, the displacement fields obtained for two de-correlation events separated by as much as 150 minutes look pretty similar. The persistence in time of the direction of the local displacement can be better highlighted by introducing the angular correlation of the "director" $\langle \cos\theta(\tau)\rangle = \langle \Delta\mathbf{r}(0)\cdot\Delta\mathbf{r}(\tau)\rangle$, where the average is performed over all the ROIs, which quantifies how much the direction of a local displacements change in time. The bottom-left panel in Fig. 6 shows that these angular correlation persist over a very long time scale. Averaging over the local vector displacements also allows to evaluate the overall r.m.s. displacement $\Delta r(t) = \langle \Delta x^2(t) + \Delta y^2(t)\rangle^{1/2}$ of the gel. The bottom-right panel of Fig. 6 shows that that the time-dependence $\Delta r(t)$ exhibits two distinct regimes at short and long time, both described by a power law, but with an exponent $\alpha_s \simeq 0.46$ at short time, and $\alpha_l \simeq 0.87$ at longer time, respectively suggesting a diffusive and a quasi-ballistic process. Notice that, reassuringly, α_l^{-1} is almost coincident with the exponent of the "compressed" exponential observed for $g_2(\tau;t)$ at large q[+]. Our evidence suggests that

[+] It is also useful to point out that the transition between the two regimes takes places for a value of $\Delta r(t) \simeq 3\,\mu$m corresponding to a q-vector which is larger than the upper limit of the q-range our setup can probe. This further highlight the usefulness of real-space analysis.

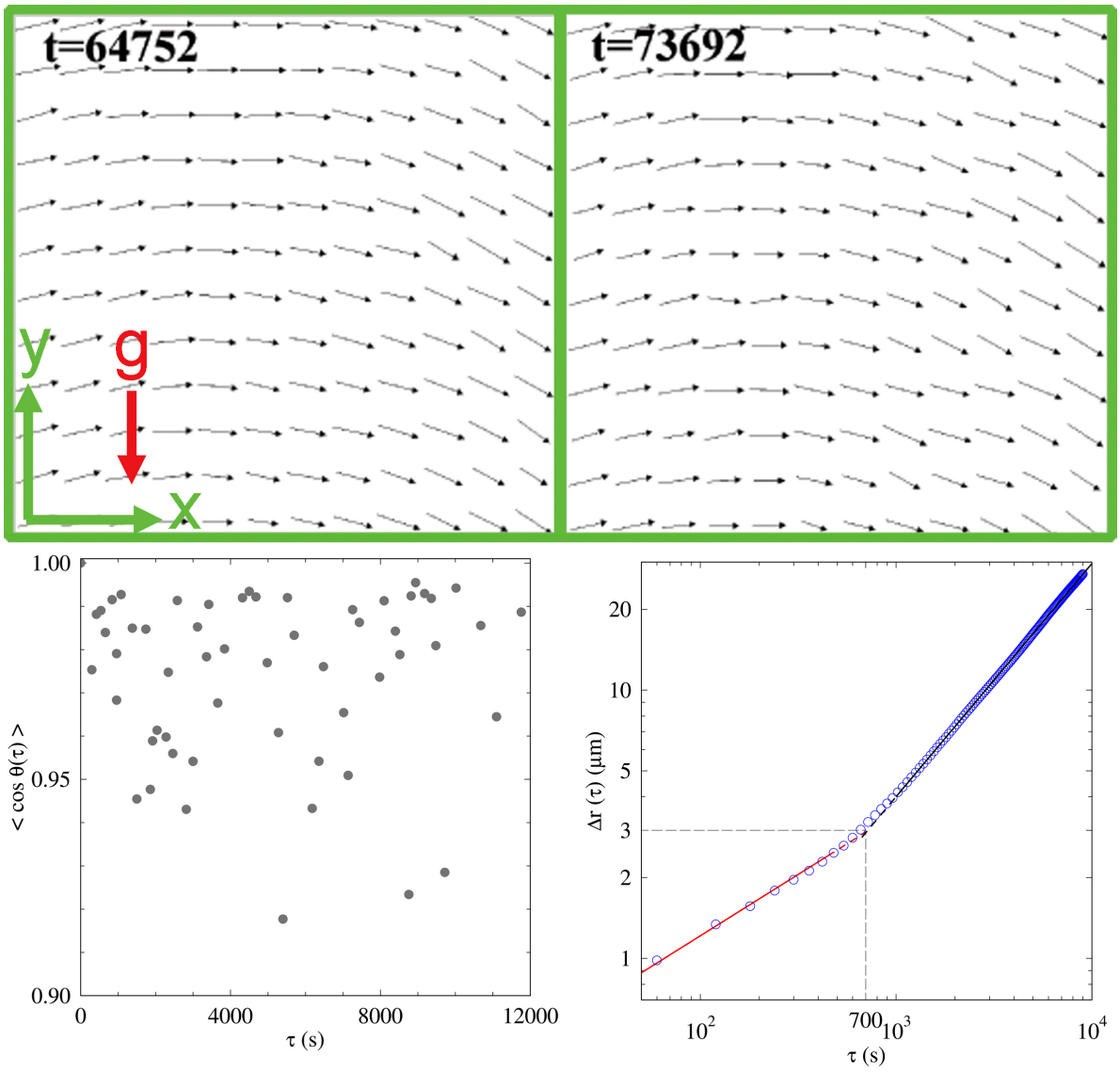

Figure 6. Top: Normalized displacement fields at two different times, indicated in the legend, where de-correlation burst are observed. Bottom left: angular correlation in time of the normalized displacement vector at a fixed location, where the average is performed over the 144 ROIs. Bottom right: Overall root-mean-square displacement of the gel as a function of time. The full lines are power-law fits to the short and long time behavior, with exponents $\alpha_s = 0.4$ and $\alpha_l = 0.8$ respectively.

deviations from a purely ballistic motion are small, which allows to define an average velocity. Notably, the values of this average velocity respectively obtained by Fourier analysis of the data in Fig. 3 ($v_F = \langle 1/(q\,\langle\tau\rangle)\rangle \simeq 1.5 \times 10^{-3}\,\mu\mathrm{m\,s^{-1}}$) and from real space analysis of the images in Fig. 6 ($v_r = \lim_{\tau\to\infty} \Delta r(\tau)/\tau \simeq 2.8 \times 10^{-3}\,\mu\mathrm{m\,s^{-1}}$) have the same order of magnitude, which further strengthens the overall agreement between the two approaches. All the evidence we found is thus consistent with a model where the loss of correlation is due to "quasi-ballistic" processes, where subsequent displacements add on coherently.

6. Discussion

In this work, we have studied the spatially heterogeneous dynamics of a strong gel obtained by irreversible colloidal aggregation using Digital Fourier Imaging in a bright-field configuration. The experimental evidence we have collected shows that the reciprocal-space information digitally recovered from DFI data provides results that are fully consistent with those previously obtained either by traditional small-angle static and dynamic light scattering [1, 3], or by more recent optical correlation techniques like Time-Resolved Correlation [6]. Specifically, in the earliest stages of aggregation $S(q)$, besides witnessing the fractal structure of the aggregating clusters, is characterized by the occurrence of a "diffusion hole" at small q-vectors, similar to the one observed in spinodal decomposition processes. Once the system has formed a space-filling gel network, however, this hole fills progressively up, so that during the later ageing stage the gel is characterized by a monotonically increasing of $S(q)$. Such a structural evolution is accompanied by substantial changes in the dynamics, which can be investigated by analyzing the degree of temporal correlation between two images acquired at time difference τ. At a given ageing time t, the mechanical properties of the gel depend on the time scale on which they are observed. For instance, for $t \gtrsim 2 \times 10^4$ s the gel looks fully rigid over a time scale τ of the order of a minute (apart from an initial very fast relaxation due to internal modes), but still shows consistent relaxation at much larger values of τ. As a matter of fact, over a time scales of a couple of hours, the gel still shows a fluid-like "creeping" behavior even after an ageing time of a day. This very slow, persistent relaxation is arguably the resulting effect of the stockpiling of a large number of microscopic local rearrangement processes, evidenced by sudden de-correlation bursts superimposing on the overall behavior of the correlation index $c^i(\tau; t)$. These fast rearrangements affect also the shape of the whole time-correlation functions $g(q, \tau)$, which relax over long times as a compressed exponential.

As we mentioned, all these features of colloidal irreversible gelation have been already and extensively investigated by light scattering and other optical correlation methods. Yet, novel information concerning the strength and spatial distribution of the microscopic rearrangements leading to the decay of gel temporal correlations can be obtained by exploiting the real-space visualization capability of DFI techniques. In particular, the observation of strikingly long spatial correlations in the local displacement field, of the temporal persistence in direction of the local displacement vectors over consecutive rearrangements, of a ballistic r.m.s. displacement at sufficiently long time, further support the model presented on the basis of PCI measurements by Duri *et al.* [12], based on assuming that consecutive events originate from the same stress source, which requires several events to fully relax. We stress again that detecting these features requires a field of view far too large to be accessible to standard video microscopy, which requires imaging and tracking the single particles in the gel. Although the evidence we collected should be regarded as preliminary and deserving further studies, the results we obtained pave the way for a systematic investigation of

the spatially heterogeneous dynamics observed for a large class of arrested structures displaying aging and temporally intermittent dynamics that, besides colloidal and polymer gels and glasses [26], includes in particular foams, which PCI studies [12] suggest to display, at variance with strong gels, short-range spatial correlations of the microscopic rearrangement events.

Acknowledgments

We thanks Luca Cipelletti, Roberto Cerbino, and Fabio Giavazzi for several interesting discussions, and acknowledge the Italian Ministry for Education, University and Research (MIUR) for funding through the projects "Futuro in Ricerca Project Anisoft/RBFR125H0M", and PRIN 2012, Project Identifier 20122HCMHJ, and ASI (Solidification of Colloids in Space) is gratefully acknowledged.

References

[1] M. Carpineti and M. Giglio. *Phys. Rev. Lett.*, 68(22):3327, 1992.
[2] A. H. Krall and D. A. Weitz. *Phys. Rev. Lett.*, 80:778–781, 1998.
[3] L. Cipelletti, S. Manley, R. C. Ball, and D. A. Weitz. *Phys. Rev. Lett.*, 84:2275–2278, 2000.
[4] L. Cipelletti, H. Bissig, V. Trappe, P. Ballesta, and S. Mazoyer. *J. Phys: Cond. Matt.*, 15:S257, 2003.
[5] W. van Megen, T. C. Mortensen, S. R. Williams, and J. Müller. *Phys. Rev. E*, 58:6073–6085, 1998.
[6] A. Duri and L. Cipelletti. *Europhys. Lett.*, 76(5):972, 2006.
[7] L. Cipelletti, L. Ramos, S. Manley, E. Pitard, D.A. Weitz, E.E. Pashkovski, and M. Johansson. *Farad. Discuss.*, 123:237–251, 2003.
[8] B. Abou, D. Bonn, and J. Meunier. *Phys. Rev. E*, 64:021510, 2001.
[9] N.B. Simeonova and W.K. Kegel. *Phys. Rev. Lett.*, 93:035701, 2004.
[10] A. Knaebel, M. Bellour, J.P. Munch, V. Viasnoff, F. Lequeux, and J.L. Harden. *Europhys. Lett.)*, 52(1):73, 2000.
[11] O. Lieleg, J. Kayser, G. Brambilla, L. Cipelletti, and A.R. Bausch. *Nat. Mater.*, 10(3):236–242, 2011.
[12] A. Duri, D.A. Sessoms, V. Trappe, and L. Cipelletti. *Phys. Rev. Lett.*, 102(8):085702, 2009.
[13] S. Mazoyer, L. Cipelletti, and L. Ramos. *Phys. Rev. Lett.*, 97:238301, 2006.
[14] F. Giavazzi and R. Cerbino. *J. Opt.*, 16(8):083001, 2014.
[15] M. Giglio, M. Carpineti, A. Vailati, and D. Brogioli. *Appl. Opt.*, 40:4036, 2001.
[16] F. Ferri, D. Magatti, D. Pescini, M. A. C. Potenza, and M. Giglio. *Phys. Rev. E*, 70:41405, 2004.
[17] R. Cerbino and V. Trappe. *Phys. Rev. Lett.*, 100:188102, 2008.
[18] S. Buzzaccaro, E. Secchi, and R. Piazza. *Phys. Rev. Lett.*, 111:048101, 2013.
[19] E. Secchi, T. Roversi, S. Buzzaccaro, L. Piazza, and R. Piazza. *Soft Matter*, 9:3931, 2013.
[20] R. Cerbino, L. Peverini, M.A.C. Potenza, A. Robert, P. Bösecke, and M. Giglio. *Nat. Phys.*, 4(3):238–243, 2008.
[21] M. D. Alaimo, M. A. C. Potenza, M. Manfredda, G. Geloni, M. Sztucki, T. Narayanan, and M. Giglio. *Phys. Rev. Lett.*, 103:194805, 2009.
[22] P.J. Lu, F. Giavazzi, T.E. Angelini, E. Zaccarelli, F. Jargstorff, A.B. Schofield, J.N. Wilking, M.B. Romanowsky, D.A. Weitz, and R. Cerbino. *Phys. Rev. Lett.*, 108:218103, 2012.
[23] E. Secchi, S. Buzzaccaro, and R. Piazza. *Soft Matter*, 10:5296–5310, 2014.

[24] M. D. Alaimo, D. Magatti, F. Ferri, and M. A. C. Potenza. *Appl. Phys. Lett.*, 88(19):191101, 2006.

[25] R. Piazza. Optical correlation techniques for the investigation of colloidal systems. In Elsevier, editor, *Colloidal Foundations of Nanoscience*, chapter 8. Elsevier, Amsterdam, 2004.

[26] L. Cipelletti and E.R. Weeks. Glassy dynamics and dynamical heterogeneity in colloids. In L. Berthier, G. Biroli, J.P. Bouchaud, L Cipelletti, and W van Saarloos, editors, *Dynamical heterogeneities in glasses, colloids, and granular media*, chapter 4. Oxford University Press, 2011.